New Journal of Physics

The open access journal at the forefront of physics





PAPER • OPEN ACCESS

Revealing the loss mechanisms of a 3D superconducting microwave cavity for use in a dark matter search

To cite this article: J C Esmenda et al 2025 New J. Phys. 27 105005

View the article online for updates and enhancements.

You may also like

- <u>Thermodynamic decoupling in the deepstrong coupling regime</u> Stephania Palafox, Mariana Salado-Mejía, Moroni Santiago-García et al.
- Averaged Disturbing Function for the Saturn-Titan-Hyperion 4:3 Resonance Letícia Guimarães Silva
- Committed acceleration of climate stresses in the coming decades Noah S Diffenbaugh

New Journal of Physics

The open access journal at the forefront of physics



Published in partnership with: Deutsche Physikalische Gesellschaft and the Institute of Physics



PAPER

OPEN ACCESS

RECEIVED

7 May 2025

REVISED

3 October 2025

ACCEPTED FOR PUBLICATION

13 October 2025

PUBLISHED

23 October 2025

Original Content from this work may be used under the terms of the Creative Commons Attribution 4.0 licence.

Any further distribution of this work must maintain attribution to the author(s) and the title of the work, journal citation and DOI.



Revealing the loss mechanisms of a 3D superconducting microwave cavity for use in a dark matter search

J C Esmenda¹, E A Laird¹, I Bailey¹, N Du², S Durham², G Carosi², T Gamble³, P Smith³, E Daw³ and Yu A Pashkin^{1,*}

- Department of Physics, Lancaster University, Lancaster LA1 4YB, United Kingdom
- ² Lawrence Livermore National Laboratory, Livermore, CA 94550, United States of America
- ³ School of Mathematical and Physical Sciences, University of Sheffield, Sheffield S3 7RH, United Kingdom
- * Author to whom any correspondence should be addressed.

E-mail: y.pashkin@lancaster.ac.uk and j.esmenda@lancaster.ac.uk

Keywords: superconducting microwave cavity, quality factor, loss mechanisms, dark matter search Supplementary material for this article is available online

supplementary material for this article is available offin

Abstract

Superconducting microwave cavities have found applications in many areas including quantum computing, particle accelerators, and dark matter searches. Their extremely high quality factors translate to very narrow bandwidth, which makes them key components of sensitive detectors. In this study, we aim to understand the loss mechanisms of an aluminium cavity, with a fundamental mode frequency of about 2.5123 GHz, and how they change as the cavity material transitions from the superconducting to normal state. We found that at temperatures not much lower than the transition temperature $T_{\rm c}$, losses are dominated by quasiparticle excitations and are well described by the Bardeen–Cooper–Schrieffer theory. The exponential decrease of the quasiparticle density below $T_{\rm c}$ results in a 1000-fold increase of the quality factor, as well as a shift of the resonance frequency due to the change of the kinetic inductance of the superconductor. At very low temperatures, losses due to two-level systems begin to dominate giving a peak in the quality factor of about 2.76×10^7 at 130 mK. Understanding the loss mechanisms is invaluable, as the working temperature of the cavity may vary during operation regardless of its application.

1. Introduction

The ability of a superconducting microwave cavity to retain a large amount of energy compared to how much power it loses per cycle is the fundamental basis of its value as a key component in a number of important research areas. These include particle physics, where the mature technology of superconducting radio-frequency cavities is used for accelerators [1], and quantum computing [2-4], where long coherence times are vital for robust quantum information processing and error correction. This paper focuses on the application of such cavities to dark matter searches. The use of three-dimensional (3D) microwave cavities for light dark matter searches was first proposed [5, 6] and realised [7, 8] in the 1980s, and continued by the ADMX collaboration at the start of the century [9, 10]. In recent years a large number of other experiments of this kind have been proposed. The majority of these are axion haloscopes featuring a resonant microwave structure immersed in a strong, static magnetic field. This field enables the conversion of hypothetical axion dark matter to photons, and the most common resonant structure used to enhance the photon signal is a cylindrical cavity. Axion conversion is then searched for by measuring the power contained in the modes of the cavity, where the fundamental transverse magnetic (TM) mode (TM₀₁₀) is typically the most sensitive. This is because the TM₀₁₀ mode in the cylindrical cavity maximises the overlap between the electric field of the cavity and the effective current induced by the axion field over the volume of the cavity, assuming that the external magnetic field is uniform and coaxial with the cavity. The requirement of an external magnetic field makes the use of superconducting cavities challenging, but the use of type II superconductors for this purpose has

been demonstrated [11, 12]. A superconducting cavity can also be used to probe the cold dark matter paraphoton-photon coupling, as this does not require a magnetic field. Such experiments can either be sensitive to dark matter paraphotons using a haloscope geometry as in the axion case discussed above, or else both produce and detect hypothetical paraphotons using a 'light shining through a wall' geometry [13–18]. The advantage of superconducting cavities is due to the very low resistive loss the cavity wall achieves when the material turns superconductor, sustaining standing waves inside it before leaking energy. In other words, the ratio of the energy stored inside the cavity over the energy lost during one radian of oscillation, more commonly referred to as its quality factor, becomes extremely high. This then translates to very narrow bandwidths, which are an important feature of sensitive detectors. In practice, however, the expected high quality factor values are not always achieved. This suggests that there are other loss mechanisms that persist even when the cavity is superconducting [3, 19–22]. For this reason, it is imperative to understand how these different loss mechanisms occur and behave if one is to maximise the efficacy of this technology.

To this end, we characterise an aluminium cavity with a cylindrical geometry, developed as part of the ADMX collaboration's experimental programme, in its superconducting temperature range. We then explore how losses due to surface imperfections in 3D cavities are minimised with the aid of simulations. More importantly, we try to understand temperature dependent losses and how they contribute to the overall observed quality factor. While detailed studies of losses have been carried out on 3D superconducting cavities of different geometries [23–27], a careful study of the losses for this geometry is of particular interest to the dark matter search community. Moreover, the insights learned in this study will be an important addition to the knowledge base of superconducting cavities, in general.

2. Cavity characterisation

The cavity, which is a cylinder with an interior length and radius of 121 mm and 46.05 mm, respectively, is formed from two mirrored halves of a milled Al 6061-T6 alloy with rounded edges as illustrated in figure 1(a). To probe the cavity, two small through holes on one of the circular faces are made. It is important to note here that there are also two larger holes located on both circular faces of the cavity that are designed for a frequency tuning rod insertion but are not used for this experiment. Eight copper clamps tightened with brass screws embrace the cavity and are attached to the mixing chamber plate of a dilution refrigerator with a base temperature of 8 mK as shown in figure 1(b). Using a calculated thermal equilibration time of tens of milliseconds for a decimetre-sized volume of superconducting aluminium, a thermalisation time of at least 40 minutes in between temperature points ensures that the temperature of the cavity is approximated well by the thermometer of the plate. Transmission measurements through the cavity are done by using two copper coaxial cables, where the central line at one end protrudes by a small amount to the probe through-holes while being secured from the outside using collet screws as shown in figure 1(c). The insertion depth of the antenna is adjusted at room temperature such that the coupling to the external circuitry is minimised. Nevertheless, despite this effort, the coupling strength is expected to change at cryogenic temperatures, which may lead to increased crosstalk and parasitic effects. These issues are managed through precise model fitting and calibration. It should also be noted here that upon receiving the cavity from the manufacturer, the cavity was cleaned modestly without any chemical treatment or additional machine polishing before any assembly and measurement were performed. Even with minimal preparations, the cylindrical cavity, which has a fundamental resonance frequency f_0 of 2.5123 GHz, was measured to have a quality factor Q of 26.095×10^6 at the base temperature using a Lorentzian fit as shown in figure 1(d). This frequency corresponds to axion masses around $10 \,\mu\text{eV}\,\text{c}^{-2}$, which is in a region well-motivated by cosmology models. In practice, the frequency can be modified using a tuning rod, which is not included in this study. Details on the fitting procedure, handling of crosstalk and calibration, and the delivery of microwave signals to the cavity input, used to characterise both high $(-79 \, \text{dBm})$ and low $(-139 \, \text{dBm})$ power regimes, are provided in the supplementary file. Notably, both fits yield consistent results, indicating no significant power-dependent shift in the extracted parameters.

3. Effect of geometry on surface losses

Finite element method simulators such as COMSOL [28] allow for determining the frequencies and visualisation of the resonance modes of the cavity, and more importantly, can be used to understand the geometrical effect on losses. Table 1 summarises the measured resonance frequencies and quality factors of the different modes of the cavity. In the same table, the corresponding simulated frequencies are then

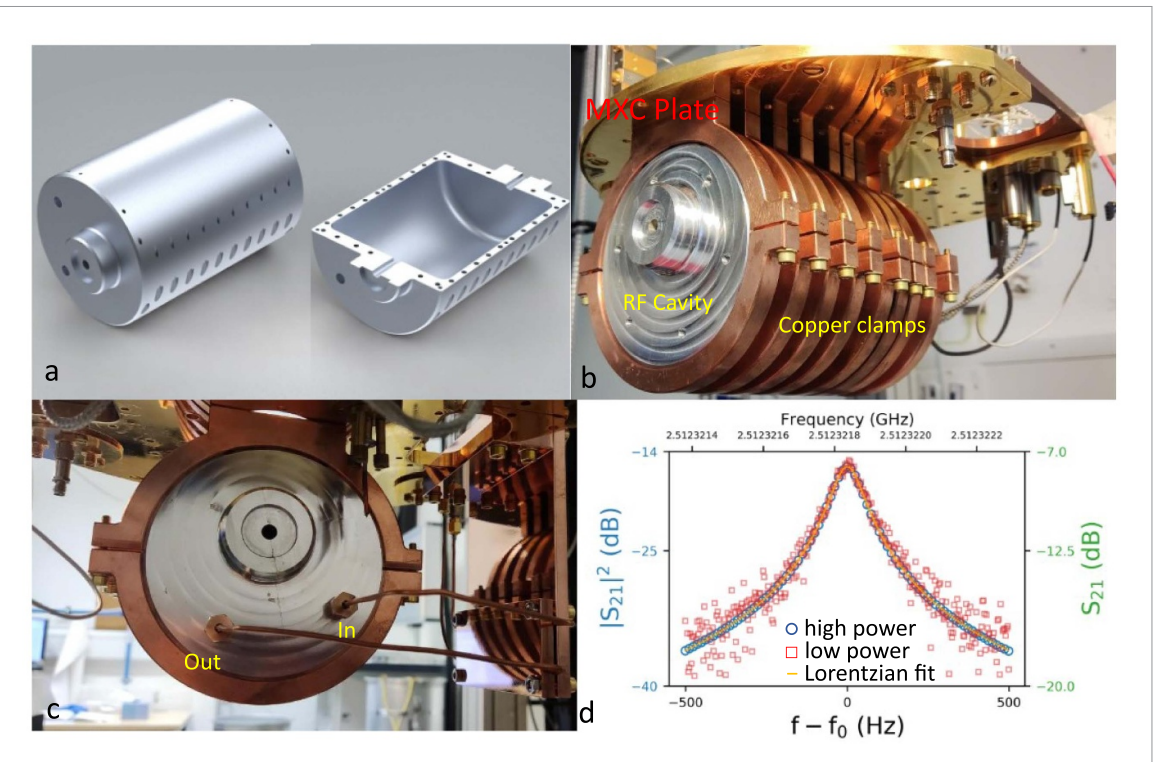


Figure 1. (a) Renders of the measured cavity. (b) Aluminium cylindrical cavity clamped to the mixing chamber plate using copper brackets tightened with brass screws. (c) Copper feedthroughs are secured to the cavity using collet screws. (d) Transmission of the TM₀₁₀ mode of the cavity with a high (blue circles) and low power (red squares) input and corresponding Lorentzian fit (orange line).

calculated using the COMSOL model. It is important to mention that the model does not include asymmetry effects, which may arise from geometric eccentricity or the presence of probes. The mode names in the first column of table 1 indicate whether the mode is transverse electric (TE) or TM while the succeeding numbers represent the nodal indices for the azimuthal, radial, and transverse degrees of freedom with the subscripts a and b designating modes with the same nodal indices but split due to asymmetry. Visualisation of the corresponding modal volumes of the electrical fields of these resonances shown in figure 2 help us understand why, for example, no peak is observed for the TE₁₀₁ mode. This is due to the transmission antenna being located in a low-field region of TE₁₀₁ and perpendicular to the electric field lines. This makes TM₀₁₀ the lowest observed mode in this experiment. It is also the mode of most interest to the majority of light dark matter searches. It is important to mention here as well that seam loss is minimised by using TM₀₁₀ mode in this case because the current flows in the same direction as the seam. To see the geometrical effect on losses, we begin by understanding surface imperfections.

Surface imperfections for a three dimensional cavity account for two types of losses, which ultimately determine its quality factor. The first type comes from the oxide layer at the surface, characterised by a dielectric loss tangent $\tan \delta$ or $1/\tan \delta = Q_{\rm diel}$ in terms of Q. To estimate the actual Q due to this loss, one needs to calculate the dielectric participation $P_{\rm diel}$. By summing up the electric field for the cavity's interior surface area S and interior volume V and taking the ratio, the dielectric participation can be calculated by the following equation:

$$P_{\text{diel}} = \frac{\varepsilon_{\text{r}} t \iint |\vec{E}|^2 dS}{\iint \iint |\vec{E}|^2 dV},$$
(1)

where t and ε_r , are the thickness and relative permittivity, respectively. With this, surface oxide Q will be $Q_{\rm int,E} = Q_{\rm diel}/P_{\rm diel}$ [29]. Using COMSOL, the dielectric participation can be estimated for the different modes for an oxide thickness t=3 nm as shown in table 1 [30]. From these values, one can see that the dielectric participation values for the cavity modes of this geometry are very low. As an example, using the calculated dielectric participation for TM_{010} , $Q_{\rm int,E}$ can be as high as 10^{11} (for $\tan\delta=0.0001$) [22]. This is further reinforced by the independence of the fundamental response peak on the input power as opposed to planar resonators, where the presence of oxide lead to power dependent frequencies and lifetimes [19].

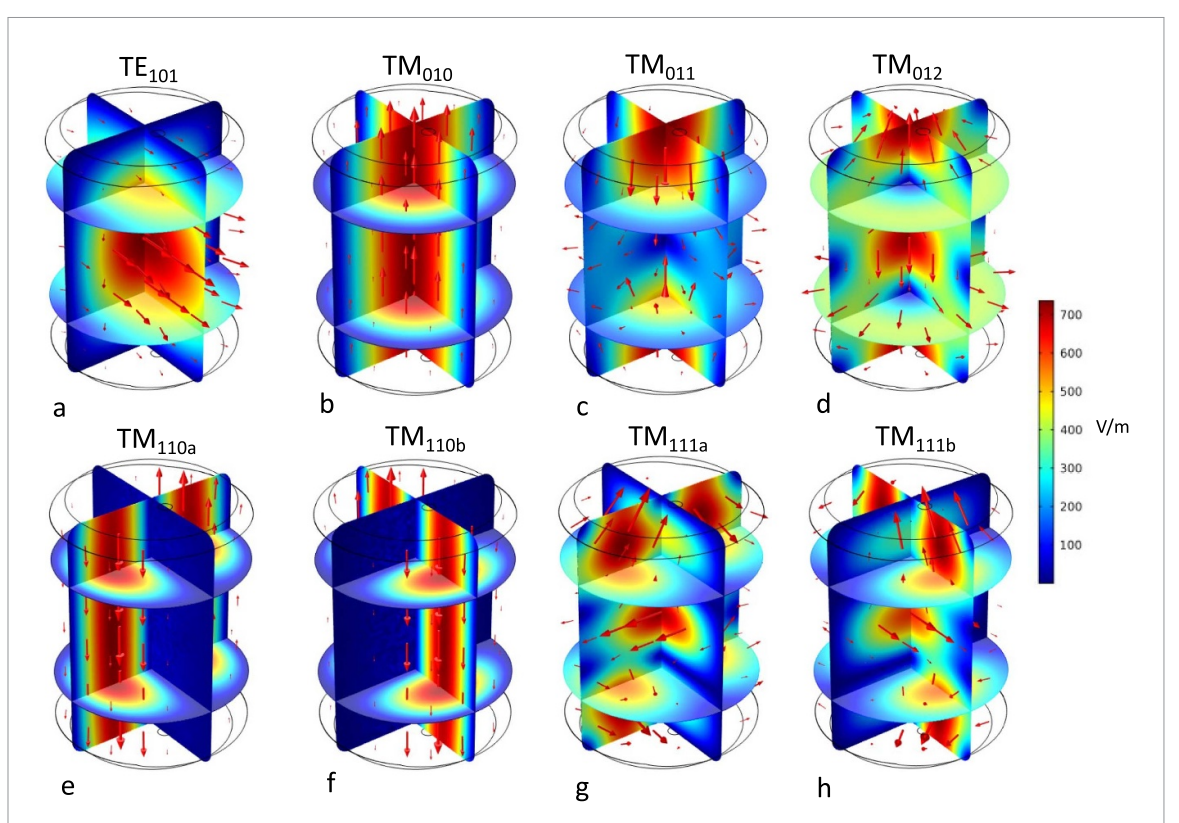


Figure 2. Visualisation of the different modes from the model, where the slices show the electric field magnitude heat map and the arrows indicate the electric field direction.

The second surface loss is due to the surface resistance R_s , possibly from a finite quasiparticle density. Estimating the Q due to this loss, one needs to determine the geometric factor $G(\Omega)$ [31, 32] which is given by:

$$G = \frac{\omega \mu_0 \int \int \int |\vec{H}|^2 dV}{\int \int |\vec{H}|^2 dS}$$
 (2)

for a mode angular frequency ω , vacuum permeability μ_0 , and the volume-to-surface ratio of the magnetic field H. The corresponding Q due to this surface resistance will be $Q_{\text{int},H} = G/R_s$ [33]. In other words, the geometric factor is a measure of how much surface resistance is reduced due to the cavity's shape. Similarly to the oxide losses, geometric factor values can be calculated using the model as shown in table 1. From the model, the geometric factors are in the range of several hundred Ohms, which are typical values for 3D cavities [33]. These are large values compared to two-dimensional resonators, where the geometrical values are typically below 1 [22]. Furthermore, surface resistances are calculated using the simulated geometric factors and internal quality factors extracted from throughtype measurements, where the cavity is replaced by a coaxial line, as detailed in the supplementary file. The resulting surface resistance values are presented in the final column of table 1. A close agreement is observed between the surface resistance values of the fundamental modes reported in this work and those of the 3D-printed aluminium cavities (Al-12Si) [33], once the quadratic dependence of surface resistance on frequency is taken into account in the absence of an applied magnetic field. It is important to note that surface resistance is not a fixed material quantity; rather, it depends sensitively on the fabrication method, operating frequency, temperature, presence of impurities, and surface morphology.

4. Effect of temperature on resonance shift

A shift in the fundamental frequency is observed as the cavity temperature goes from base temperature to around the superconducting transition temperature T_c as shown in figure 3(a). This shift can be explained by the dependence of the kinetic inductance L_k on temperature through the material superconducting energy gap Δ , which changes with temperature. For a resonator with an equivalent resistance R, capacitance C, and geometric inductance L_0 , the resonance frequency is dependent on the kinetic

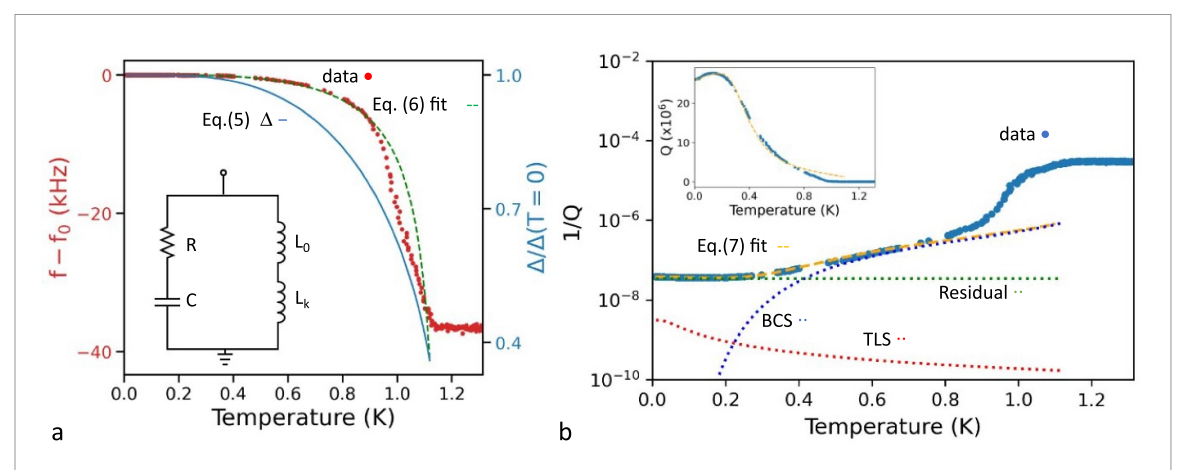


Figure 3. (a) Resonance shift of the TM_{010} mode as a function of cavity temperature and equivalent circuit (inset). The secondary axis is the superconducting energy gap normalised to its value when temperature is 0. (b) Temperature dependence of the quality factor of the TM_{010} mode (inset) and the weighted contributions of various loss mechanisms to the total loss.

inductance as [34]

$$f = \frac{1}{2\pi\sqrt{C(L_0 + L_k)}}. (3)$$

and the kinetic inductance is given by [35]

$$L_{\mathbf{k}} = \frac{R\hbar}{\pi \, \Delta \tanh \frac{\Delta}{2k_{\mathrm{B}}T}}.\tag{4}$$

In Bardeen–Cooper–Schrieffer (BCS) theory, the temperature dependence of Δ can be approximated as [36, 37]

$$\Delta(T) = 1.76k_{\rm B}T_{\rm c}\tanh\frac{\pi}{1.76}\sqrt{\frac{T_{\rm c}}{T} - 1}.$$
 (5)

The fitting equation then becomes

$$f(T) = \left(\delta + \frac{\epsilon}{F}\right)^{-1/2},\tag{6}$$

where $E = \Delta \tanh(\Delta/2k_BT)$, $\delta = 4\pi^2CL_0$, and $\epsilon = 4\pi\hbar CR$. Here, δ and ϵ are fitting parameters and \hbar and k_B are Planck's and Boltzmann's contants, respectively. Another consideration is frequency shifts induced by changes in quality factor, such as shifts due to two-level systems (TLS) [38]. These changes are minimal, however, as approximated by $-f2\pi/8Q^2$ [39], which results in values typically on the order of a few hertz for this experiment. By setting T_c to 1.17 K [40], the model produced a good fit as shown in figure 3(a), which yields parameter values $\delta = 1.5846135 \times 10^{-19} \text{ s}^2$ and $\epsilon = 2.79 \times 10^{-47} \text{ Js}^2$. Using these two fitting parameters, we obtain $R/L_0 = \pi \epsilon/\hbar \delta = 5.2 \times 10^6 \, \mathrm{s}^{-1}$. The equivalent resistance R is in fact the surface resistance R_s of the superconductor. With the value of R_s for the TM₀₁₀ mode from table 1 and equation (4), we obtain the kinetic inductance fraction $L_k/(L_0 + L_k) = 6.2 \times 10^{-6}$, which agrees well with the reported values [23, 24]. The overall behaviour of the resonance frequency shift with respect to temperature very much resembles the temperature dependence of Δ described by the phenomenological expression presented in equation (5), which has almost no dependence when T is close to zero and then makes a sharp and abrupt fall as T approaches T_c. It should be noted, however, that this approach is less accurate than the Matthis-Bardeen method, as evidenced by the discrepancy between the fit and all data near T_c . Nevertheless, it provides an expression that can be linearly combined with other loss mechanisms as will be demonstrated in the following section.

New J. Phys. 27 (2025) 105005 J C Esmenda et al

Table 1. Extracted cavity values for the different modes from the experiment and simulations.

Mode	Measured Freq. (GHz)	Measured Q Factor $(\times 10^6)$	Simulated Freq. (GHz)	Dielectric ^a Participation P_{diel}	Geometric Factor $G(\Omega)$	Surface Resistance R_s ($\mu\Omega$)
TE ₁₀₁	N/A	N/A	2.2866	5.48×10^{-7}	309	N/A
TM_{010}	2.5123	26.095	2.5118	4.76×10^{-7}	342	12.2
TM_{011}	2.8156	22.086	2.8155	1.03×10^{-6}	306	13.2
TM_{012}	3.5571	23.599	3.5548	1.14×10^{-6}	384	15.6
TM_{110a}	4.0007	24.730	4.0012	4.44×10^{-7}	551	20.0
TM_{110b}	4.0025	0.066	4.0012	4.47×10^{-7}	550	4790
TM_{111a}	4.2245	25.438	4.2232	6.74×10^{-7}	582	21.2
TM_{111b}	4.2248	8.892	4.2232	7.58×10^{-7}	546	57.4

Notes: ^aEstimate for an oxide layer of thickness t = 3 nm.

5. Effect of temperature on quality factor

Figure 3(b) shows how the quality factor of the fundamental mode changes as the temperature decreases from T_c to the base temperature. This behaviour of the quality factor can be seemingly described in two temperature ranges. One is from T_c to around 220 mK and the other is from 220 mK to the base temperature. In the first range, there is about a thousand fold change of the quality factor. On the other hand, the second range, while there is not much change in the value of Q, a small but noticeable peak occurs at about 130 mK, where the quality factor reached about 27.6 million. This two-range description seemingly hints to two temperature dependent loss mechanisms. As it turns out, there are two mechanisms that behave differently with temperature. These are the surface resistance predicted by the BCS theory [41] and the losses due to TLS [42]. These losses have different origins and therefore behave differently with temperature change. BCS losses come from the heating of unpaired electrons whose number increases with temperature. This resistance is dependent on temperature with the expression $\exp(-\Delta/(k_BT))/T$ [31]. TLS losses, on the other hand, as the name suggests, stem from microscopic objects within the cavity wall that have two distinct energy levels, creating a quantum system where atoms can tunnel between these energy minima. These objects can be from any impurities, such as non-aluminium elements that are present in the alloy, or any other defects and dislocations in the lattice structure. TLS losses depend on temperature with the expression $\tanh(\hbar\omega/(2k_BT))$ [21, 26]. Using these two expression, we can create a model that can describe the behaviour of the quality factor over the aforementioned two temperature ranges as

$$\begin{split} \frac{1}{Q_{\text{total}}} &= \frac{1}{Q_{\text{BCS}}} + \frac{1}{Q_{\text{TLS}}} + \frac{1}{Q_{\text{residual}}} \\ &= \alpha \frac{\exp\left(-\frac{\Delta}{k_{\text{B}}T}\right)}{T} + \beta \tanh\frac{\hbar\omega}{2k_{\text{B}}T} + \gamma, \end{split} \tag{7}$$

where α , β , γ are the fitting factors for BCS losses, TLS losses, and any other residual losses that are not dependent on temperature, respectively. Using the same $T_c = 1.17\,\mathrm{K}$ for the resonance shift model, and Q(0) = Q at base temperature, a reasonable fit was produced using this model shown in figure 3(b), which yields parameter values $\alpha = 1.8795 \times 10^{-6}\,\mathrm{K}$, $\beta = 3.1234 \times 10^{-9}$, and $\gamma = 3.5211 \times 10^{-8}$. As mentioned earlier, while the Matthis–Bardeen method gives a more precise description of BCS-related losses, particularly near T_c , the approach used here allows for the accounting of multiple loss mechanisms and the analysis of their individual influence on the total quality factor. To further understand the contributions from various loss mechanisms, we plot each weighted contribution separately as shown in figure 3(b).

Around T_c , it is clear that the dominant contribution comes from BCS losses, which are about 25 times larger than the residual losses. BCS losses steadily decrease as the cavity temperature approaches about 300 mK and then sharply drop afterwards as the temperature approaches base temperature. TLS losses, on the other hand, increase by about 20 times gradually from 10^{-10} at T_c all the way down to base temperature. The aforementioned temperature range boundary at 220 mK is the point, in fact, at which the crossing of the two loss contributions occurs. The combination of these two behaviours explains the peak observed at around 130 mK. Interestingly, while BCS and TLS losses explain the behaviour of Q with temperature, they are not the dominant contributor of losses in the experiment. Residual losses have the largest weight at about 92% at base temperature. From the through

measurements, the coupling Q is calculated to be 5×10^8 , leading to the unaccounted internal Q to be 2.7532×10^7 . A possible source of this internal Q is the loss from the presence of dielectric. However, as discussed earlier, even increasing either the oxide thickness from 3 nm or introducing surface roughness to increase surface participation of the electrical field, this is not enough to account for this magnitude of loss. A further possible loss source is trapped flux from external magnetic fields. Due to the practical challenges of adding magnetic shielding, primarily because of the large support brackets, the Earth's magnetic field may lead to trapped flux, which could limit the quality factor to values of order 10^7 – 10⁸ [43]. Another possible cause of loss could be the presence of the tuning rod holes. Firstly, energy from inside the cavity can leak out through these holes and, secondly, quasiparticles can be excited by external radiation entering the cavity through these holes. The former can be estimated by $\exp(-4\pi z/r)$ for the fraction of power that is lost through a circular waveguide of radius r and length z when $r \ll \lambda$, where λ is the radiation wavelength [44]. The estimated power reduction for the fundamental mode is about 5.2×10^{-39} for a r = 3.183 mm and z = 22.5 mm for the two holes, which is much lower than the measured residual losses. To verify whether quasiparticle excitation by the incoming radiation can explain the residual losses, we repeated the experiment with both holes patched by an adhesive copper foil with a conductive glue. The fact that the Q factor did not change rules out this effect as a possible cause. Hence, the residual losses are most likely caused by the presence of impurities in the cavity material. According to the alloy specifications [45], the material is composed of 95.85% aluminium and a few other elements, the dominant impurities being magnesium (1.0%) and silicon (0.6%). Understanding of exact loss mechanisms caused by different impurities can be a topic of further studies.

6. Conclusion

In summary, we have characterised an aluminium cylindrical cavity at its superconducting temperature range. Using finite element method simulations, we were able to understand how the geometry of 3D cavities results in very low surface participation of both dielectric losses and surface resistance, leading to theoretically extremely high Q values. In practice, understanding the effect of temperature on Q starts with seeing the effect of the temperature on the superconducting energy gap. This effect is clearly seen in the sharp resonance frequency shift with temperature near T_c , where the change in the superconducting energy gap affects the kinetic inductance of the cavity. Finally, the temperature dependence of Q can be described as a combination of BCS and TLS losses, where BCS contributions dominate near T_c and TLS losses become more prominent at temperatures near zero. This mixture of behaviour results in a small peak in Q. Remarkably, through this experiment we learned that we can achieve a high internal Q even with a cavity material with a lot of impurities. This means that by using three dimensional superconducting cavities with smooth wall transitions such as this cavity, it allows you to have the best ceiling of Q values while also having the best baseline of low losses due to surface imperfections as compared to cavities of other geometries. In the context of light dark matter searches, type I superconducting cavities such at the one characterised in this study can be deployed in the search for paraphotons where an external magnetic field is not required, and the signal power directly scales with the quality factor of the cavity. For axion searches, such a cavity may still be suitable if higher order modes of the cavity are exploited and a heterodyne approach is used [46] such that the magnetic field is provided by the resonant modes of the cavity itself. The sensitivity of axion haloscopes can be compared by considering the smallest value of the effective axion-photon coupling constant that would lead to a detectable signal. This value roughly scales with the quality factor of the cavity to the power of -1/2. In earlier studies of axion haloscopes [6], it was concluded that increasing the quality factor of the cavity much above 10⁶ would be of limited advantage due to the effective quality factor of the axion field itself originating in its velocity spread. More recent studies [47], however, show that measurement rate can potentially be increased by improving the cavity quality factor to the levels demonstrated in this paper. Overall, this analysis and understanding of these loss mechanisms will be important to any area this technology is applied.

Data availability statement

The data that support the findings of this study are available upon reasonable request from the authors.

Acknowledgments

We thank the ADMX group members who designed the cavity and Eroda Ltd [48]. who manufactured it. We also thank Sam Furness for his contributions to the measurements and data analysis. The

Lancaster and Sheffield groups acknowledge the support of the Science and Technology Facilities Council (STFC) with the Quantum Sensors for the Hidden Sector (QSHS) project (ST/T006102/1), ParaPara project (ST/W006502/1), and the European Research Council (Grant 824109). The LLNL group is supported by the U.S. Department of Energy under Contract DE-AC52-07NA27344. LLNL-JRNL-2008838.

ORCID iDs

```
J C Esmenda  0009-0004-8750-4179
E A Laird D 0000-0001-9589-127X
G Carosi D 0000-0003-0130-6979
E Daw 0000-0002-3780-5430
Yu A Pashkin D 0000-0003-4767-8217
```

References

- [1] Padamsee H S 2014 Annu. Rev. Nucl. Part. Sci. 64 175-96
- [2] Blais A, Huang R S, Wallraff A, Girvin S M and Schoelkopf R J 2004 Phys. Rev. A 69 062320
- [3] Krasnok A, Dhakal P, Fedorov A, Frigola P, Kelly M and Kutsaev S 2024 Appl. Phys. Rev. 11 011302
- [4] Reagor M J 2016 Superconducting cavities for circuit quantum electrodynamics PhD Thesis Yale University
- [5] Sikivie P 1983 Phys. Rev. Lett. 51 1415
- [6] Sikivie P 1985 Phys. Rev. D 32 2988
- [7] DePanfilis S, Melissinos A, Moskowitz B, Rogers J, Semertzidis Y K, Wuensch W, Halama H, Prodell A, Fowler W and Nezrick F 1987 Phys. Rev. Lett. 59 839
- [8] Hagmann C, Sikivie P, Sullivan N and Tanner D 1990 Phys. Rev. D 42 1297
- [9] Asztalos S et al 2001 Phys. Rev. D 64 092003
- [10] Asztalos S J et al 2010 Phys. Rev. Lett. 104 041301
- [11] Alesini D et al 2019 Phys. Rev. D 99 101101
- [12] Golm J et al 2022 IEEE Trans. Appl. Supercond. 32 1-5
- [13] Jaeckel J and Ringwald A 2008 Phys. Lett. B 659 509-14
- [14] Parker S R, Rybka G and Tobar M E 2013 Phys. Rev. D 87 115008
- [15] Povey R G, Hartnett J G and Tobar M E 2011 Phys. Rev. D 84 055023
- [16] Caspers F, Jaeckel J and Ringwald A 2009 J. Instrum. 4 11013
- [17] Povey R G, Hartnett J G and Tobar M E 2010 Phys. Rev. D 82 052003
- [18] Parker S R, Hartnett J G, Povey R G and Tobar M E 2013 Phys. Rev. D 88 112004
- [19] Martinis J M et al 2005 Phys. Rev. Lett. 95 210503
- [20] Gao J 2008 The Physics of Superconducting Microwave Resonators (California Institute of Technology)
- [21] Pappas D P, Vissers M R, Wisbey D S, Kline J S and Gao J 2011 IEEE Trans. Appl. Supercond. 21 871-4
- [22] Zmuidzinas J 2012 Annu. Rev. Condens. Matter Phys. 3 169-214
- [23] Reagor M et al 2013 Appl. Phys. Lett. 102 192604
- [24] Kudra M, Biznárová J, Fadavi Roudsari A, Burnett J, Niepce D, Gasparinetti S, Wickman B and Delsing P 2020 Appl. Phys. Lett. **117** 070601
- [25] Romanenko A and Schuster D 2017 Phys. Rev. Lett. 119 264801
- [26] Romanenko A, Pilipenko R, Zorzetti S, Frolov D, Awida M, Belomestnykh S, Posen S and Grassellino A 2020 Phys. Rev. Appl.
- [27] Bafia D, Grassellino A, Checchin M, Zasadzinski J F and Romanenko A 2025 Phys. Rev. Appl. 23 054052
- [28] COMSOL (available at: www.comsol.com/products/multiphysics/)
- [29] Pozar D M 2011 Microwave Amplifier Design vol 1066 (Wiley)
- [30] Wenner J et al 2011 Appl. Phys. Lett. 99 113513
- [31] Gurevich A 2017 Supercond. Sci. Technol. 30 034004
- [32] Banford A and Stafford G 1961 J. Nucl. Energy C 3 287
- [33] Creedon D L, Goryachev M, Kostylev N, Sercombe T B and Tobar M E 2016 Appl. Phys. Lett. 109 032601
- [34] Godse A P and Bakshi U A 2020 Electronic Circuits (Technical Publications)
- [35] Annunziata A J, Santavicca D F, Frunzio L, Catelani G, Rooks M J, Frydman A and Prober D E 2010 Nanotechnology 21 445202
- [36] Gross F, Chandrasekhar B, Einzel D, Andres K, Hirschfeld P, Ott H, Beuers J, Fisk Z and Smith J 1986 Z. Phys. B 64 175-88
- [37] Poole C P, Farach H A, Creswick R J and Prozorov R 2014 Superconductivity (Elsevier)
- [38] Müller C, Cole J H and Lisenfeld J 2019 Rep. Prog. Phys. 82 124501
- [39] Hayek S I 2003 Digital Encyclopedia of Applied Physics (Wiley) [40] Faber T and Pippard A B 1955 Proc. R. Soc. A 231 336-53
- [41] Turneaure J and Weissman I 1968 J. Appl. Phys. 39 4417–27
- [42] Phillips W A 1987 Rep. Prog. Phys. 50 1657
- [43] Catelani G, Li K, Axline C J, Brecht T, Frunzio L, Schoelkopf R J and Glazman L 2022 Supercond. Sci. Technol. 35 065016
- [44] Nikitin A Y, Zueco D, García-Vidal F and Martín-Moreno L 2008 Phys. Rev. B 78 165429
- [45] Kaufman J G 2000 Introduction to Aluminum Alloys and Tempers (ASM International)
- [46] Berlin A, D'Agnolo R T, Ellis S A and Zhou K 2021 Phys. Rev. D 104 L111701
- [47] Kim D, Jeong J, Youn S, Kim Y and Semertzidis Y K 2020 J. Cosmol. Astropart. Phys. JCAP03(2020)066
- [48] Erodatools Ltd (available at: www.erodatoolsltd.co.uk) (Accessed 9 April 2025)